Isoscalar giant dipole resonance in Pb-208 via inelastic alpha scattering at 400 MeV and nuclear incompressibility

Uchida, M; Sakaguchi, H; Itoh, M; Yosoi, M; Kawabata, T; Takeda, H; Yasuda, Y; Murakami, T; Ishikawa, T; Taki, T

Published in:
Physics Letters B

DOI:
10.1016/S0370-2693(03)00137-0

Publication date:
2003

Available online at www.sciencedirect.com
SCIENCE DIRECT®
PHYSICS LETTERS B
ELSEVIER
Physics Letters B 557 (2003) 12–19
www.elsevier.com/locate/npe

Isoscalar giant dipole resonance in ^{208}Pb via inelastic α scattering at 400 MeV and nuclear incompressibility

M. Uchida [a], H. Sakaguchi [a], M. Itoh [a], M. Yosoi [a], T. Kawabata [a], H. Takeda [a], Y. Yasuda [a], T. Murakami [a], T. Ishikawa [a], T. Taki [a], N. Tsukahara [a], S. Terashima [a], U. Garg [b], M. Hedden [b], B. Kharraja [b], M. Koss [b], B.K. Nayak [b], S. Zhu [b], M. Fujiwara [c,d], H. Fujimura [c], K. Hara [c], E. Obayashi [c], H.P. Yoshida [c], H. Akimune [e], M.N. Harakeh [f], M. Volkerts [f]

[a] *Department of Physics, Kyoto University, Kyoto 606-8502, Japan*
[b] *Physics Department, University of Notre Dame, Notre Dame, IN 46556, USA*
[c] *Research Center for Nuclear Physics, Osaka University, Osaka 567-0047, Japan*
[d] *Advanced Science Research Center, Japan Atomic Energy Research Institute, Tokai 319-1195, Japan*
[e] *Department of Physics, Konan University, Kobe 658-8501, Japan*
[f] *Kernfysisch Versneller Instituut, 9747 AA Groningen, The Netherlands*

Received 17 June 2002; received in revised form 22 December 2002; accepted 30 January 2003

Editor: V. Metag

Abstract

The isoscalar giant dipole resonance (ISGDR) in ^{208}Pb has been investigated with inelastic α-scattering of 400 MeV at extremely forward angles, including 0°. Energy spectra, virtually free from instrumental background, have been obtained and the ISGDR strength distribution has been extracted using a multipole-decomposition analysis (MDA). A difference-of-spectra approach yields the same ISGDR centroid energy as with MDA. These results lead to a value for nuclear incompressibility that is consistent for both the isoscalar dipole and monopole modes.

PACS: 24.30.Cz; 21.65.+f; 24.50.+g; 27.80.+w

Incompressibility of nuclear matter has been studied experimentally and theoretically because of its fundamental importance in defining the equation of state for nuclear matter, describing various phenomena from collective excitations of nuclei to supernova explosions in the cosmos. The only direct way to experimentally determine the nuclear incompressibility is to measure the compressional-mode giant resonances, the isoscalar giant monopole resonance (ISGMR) and the isoscalar giant dipole resonance (ISGDR). Although the ISGMR has been well investigated since its discovery about 25 years ago [1,2], the location of ISGDR is still ambiguous.

E-mail address: uchida@nh.scphys.kyoto-u.ac.jp (M. Uchida).

0370-2693/03/$ – see front matter
doi:10.1016/S0370-2693(03)00137-0

Macroscopically, the ISGDR is understood as a hydrodynamic density oscillation in which a compressional wave traverses back and forth through the nucleus in the "squeezing mode" by keeping the nuclear volume constant, while the ISGMR oscillates isotropically as a "breathing mode". In the scaling model, the excitation energies of ISGMR and ISGDR are related to the nuclear incompressibility (K_A) as follows [3]:

$$E_{\mathrm{ISGMR}} \approx \sqrt{\frac{K_A}{m\langle r^2\rangle}}, \tag{1}$$

$$E_{\mathrm{ISGDR}} \approx \sqrt{\frac{7}{3}\frac{K_A + (27/25)\varepsilon_{\mathrm{F}}}{m\langle r^2\rangle}}, \tag{2}$$

where ε_{F}, m, and $\langle r^2\rangle$ are the Fermi energy, nucleon mass, and mean square radius, respectively.

Initial indications of the excitation of the ISGDR were reported as early as the beginning of the 1980s [4–6]. However, the first direct evidence for this mode, based on the differences in angular distribution of the ISGDR from that of the nearby high-energy octupole resonance (HEOR), was provided by Davis et al. [7], who demonstrated that in 200 MeV inelastic α-scattering near 0°, the giant resonance "bump" at $3\hbar\omega$ excitation energy could be separated into two components, with the higher-energy component corresponding to the ISGDR. Further evidence for the ISGDR has since come from 240 MeV inelastic α-scattering measurements on ^{90}Zr, ^{116}Sn and ^{208}Pb [8], using the multipole-decomposition (MD) technique.

One major concern with the ISGDR data so far has been that the value of the nuclear incompressibility extracted from the centroid of the ISGDR strength distribution was significantly different from that obtained from the known ISGMR energies [9]. It is now well established that the appropriate way to extract the value of the incompressibility of nuclear matter (K_{nm}) from the ISGMR energies is to compare the experimental centroids of the ISGMR with those obtained from RPA calculations with various suitable effective interactions with different K_{nm} values [10]. The problem arose when one compared the available ISGDR data with the theoretical centroids of the ISGDR, calculated using the same interactions that appear to reproduce the available ISGMR data well [11–16]. The experimental centroids reported by Clark et al. [8] were significantly lower than the calculated centroids; for example, in ^{208}Pb, Clark et al. reported the ISGDR centroid at 19.9 ± 0.8 MeV lower than previous experimental results [4–7] and also lower than theoretical values of $E_x > 22$ MeV. The low values for the centroids in the data of Clark et al. evidently resulted from their background-subtraction procedure which rendered the ISGDR strength zero at $E_x > 24$ MeV.

In this Letter, we report new measurements on the ISGDR where this apparent discrepancy between the theory and experimental data has been resolved, thanks to high quality data that allowed the extraction of the ISGDR strength up to an excitation energy of ~ 30 MeV. As described later, this has been possible because of elimination of the non-physical (instrumental) background from the final inelastic α-scattering spectra. With the results reported herein, a consistent picture emerges for the two compressional modes in ^{208}Pb, the ISGMR and ISGDR, where the experimental data on both modes can be reproduced with calculations employing the same K_{nm} value.

The present experiments have been performed at the Research Center for Nuclear Physics (RCNP), Osaka University, using inelastic α-scattering at 400 MeV and extremely forward angles, including 0°. Compared with the previous measurements at $E_\alpha \leqq 240$ MeV, the 400 MeV measurements afford several advantages; in particular, the ISGDR cross sections are significantly larger, and the contributions from pickup-breakup processes lie beyond $E_x \sim 80$ MeV. A self-supporting ^{208}Pb target of 10.1 mg/cm^2 thickness was bombarded with a 400 MeV ^{4}He^{++} beam from the RCNP ring cyclotron. Inelastically scattered particles were momentum-analyzed with the high resolution magnetic spectrometer, "Grand Raiden" [17]. The focal-plane detection system consisted of two multiwire drift chambers (MWDC) [18] and two plastic scintillation counters. Using the ray-tracing technique for the trajectories of scattered particles, energy spectra were obtained at specific angles by subdividing the full angular opening (±20 mrad) of the spectrometer. Primary ^{4}He^{++} beams were stopped at three different Faraday cups according to the setting of Grand Raiden, $\theta = 0°$, $2° < \theta < 5°$ (extremely forward angles), and $6.5° < \theta < 13°$ (ordinary forward angles). In the 0° measurements, as described in Refs. [19–21], the ^{4}He^{++} beam was guided via Grand Raiden to holes in the high-momentum side of the focal-plane

detection system, and stopped in a Faraday cup placed twelve-meters downstream from the focal plane. In measurements at extremely forward angles, however, the beam was stopped in another Faraday cup [22], which was located behind the first quadrupole magnet of the spectrometer at a distance of 155 cm from the target. In measurements at ordinary forward angles, the incident beam was stopped in a Faraday cup located inside the scattering chamber. Differential cross sections were obtained at several angles in the range of $0.64° < \bar{\theta}_{\text{c.m.}} < 13.5°$, where $\bar{\theta}_{\text{c.m.}}$ is an averaged value in the subdivided solid angle.

We utilized the vertical position spectrum at the double-focused position of the spectrometer to eliminate the instrumental background due to multiple scattering of the beam in the targets and the subsequent rescattering by the edge of the entrance slit, the yoke, and walls of the spectrometer. Inelastically scattered α-particles from "true" events are focused at the focal plane due to the ion-optics of the spectrometer, while those from background events are not focused and have a nearly flat distribution of their vertical positions. In Fig. 1(a), a vertical (y)-position spectrum at the focal plane is shown for the 0° measurement for ^{208}Pb. The spectrum has a peak from true events at $y = 0$ mm on a nearly flat background. To estimate the background in the region of true events, the spectrum gated with the background regions shown hatched on both sides of the peak was used. In Fig. 1(b), the energy spectra corresponding to gates at $-15 < y < 15$ mm and at $15 < |y| < 30$ mm (hatched) are plotted. Subtracting the spectrum associated with background from the true + background spectrum, the true spectrum with practically no instrumental background was obtained. The energy scale was calibrated using elastic and inelastic scattering of α-particles from ^{12}C (g.s., 4.439, 7.641 and 9.41 MeV states) under the same magnetic-field conditions as those in the measurements for ^{208}Pb. The energy resolution was typically 200 keV FWHM which is quite adequate for these measurements since the resonances under investigation are several-MeV wide.

Fig. 1(c) shows the 0° spectrum of ^{208}Pb(α, α') reaction after subtraction of the instrumental back-

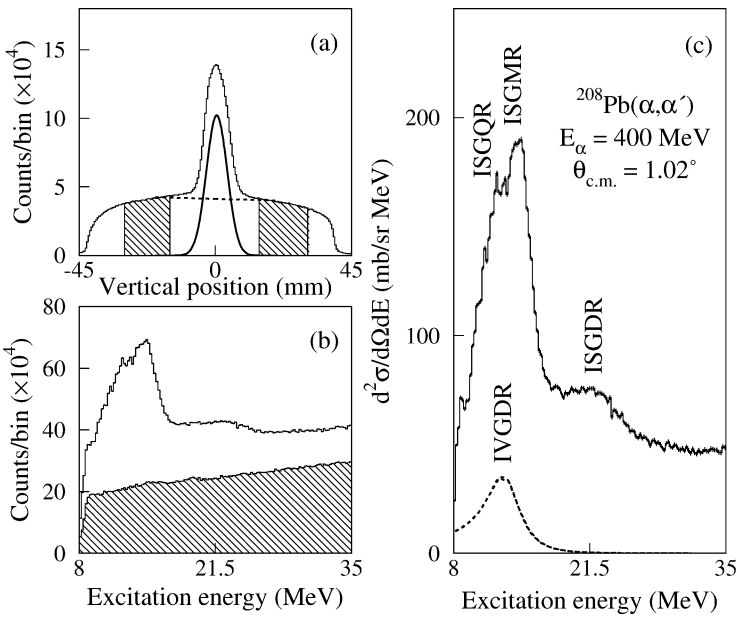

Fig. 1. (a) The vertical-position spectrum for ^{208}Pb in the 0° measurement. The spectrum has a peak from true events around $y = 0$ mm according to the focussing action of the spectrometer, while background events have trapezoidal shape. The dashed line represents background evaluated from both sides of the peak and the solid curve represents the shape of true events after subtracting the background. (b) The energy spectra gated on the region with $-15 < y < 15$ mm and $15 < |y| < 30$ mm (hatched regions). (c) Energy spectrum of the ^{208}Pb(α, α') reaction at $\bar{\theta}_{\text{c.m.}} = 1.02°$ after subtraction of background. Expected positions of the ISGQR, ISGMR and ISGDR are indicated. The contribution of the IVGDR is shown by the dashed line.

ground as described above. A prominent bump corresponding to ISGMR and the isoscalar giant guadrupole resonance (ISGQR) in ^{208}Pb is observed at $E_x \sim$ 10–15 MeV and another bump (ISGDR + HEOR) is visible at $E_x \sim 22$ MeV. In order to explore the shape of the underlying continuum at higher excitation energies, the energy spectrum at 2.2° was measured up to $E_x \sim 85$ MeV by changing the magnetic fields of Grand Raiden. The yield of the physical continuum decreases monotonically with increasing excitation energy up to $E_x \sim 60$ MeV and becomes flat thereafter. Since there is no practical or direct way to eliminate the physical continuum from the final spectra, we have performed a multipole decomposition analysis [23] of these energy spectra assuming that the continuum can be represented by a combination of higher-multipole contributions. A similar procedure has been successfully employed, for example, in (p, n) studies of Gamow–Teller giant resonances [24]. The energy spectra were sliced in 1 MeV bins and reconstructed in terms of measured angles, thus obtaining the angular distributions for each bin. Fig. 2 shows the angular distributions for two energy bins near the peaks of ISGMR and ISGDR.

The ISGDR strength distribution was obtained in two different approaches. In one of these, multipole-decomposition analysis (MDA) was used following recent analysis of giant-resonance data. In this approach, the experimental angular distribution for each energy bin was fitted with the superposition of each multipolarity as follows:

$$\left(\frac{d^2\sigma}{d\Omega\, dE}(\theta_{\text{c.m.}}, E_x)\right)^{\text{exp.}} = \sum_L a_L(E_x)\left(\frac{d^2\sigma}{d\Omega\, dE}(\theta_{\text{c.m.}}, E_x)\right)_L^{\text{calc.}}, \tag{3}$$

where $(d^2\sigma/d\Omega\, dE)_L^{\text{calc.}}$ are the calculated DWBA cross sections corresponding to 100% energy-weighted sum rule (EWSR) for each multipole at that energy, using the code ECIS95 [25]. Fitting parameters are the fractions of EWSRs, $a_L(E_x)$, which are related to the strength values, $S_L(E_x)$, as follows:

$$S_L(E_x) = m_1 \frac{a_L(E_x)}{E_x}, \tag{4}$$

where m_1 is defined as: $m_1 = \sum E_x S_L(E_x)$. Standard transition densities and deformation parameters were

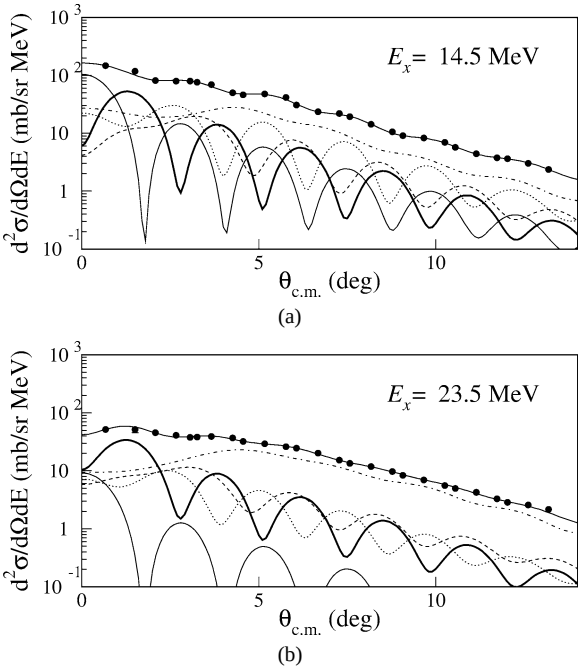

Fig. 2. Angular distributions of selected 1 MeV bins for the ^{208}Pb (α, α') reaction at 400 MeV. (a) Results for $E_x = 14.5$ MeV. The solid circles are the experimental data. The lines show contributions from $L = 0$ (thin solid line), $L = 1$ (thick solid line), $L = 2$ (dotted line), $L = 3$ (dashed line), and other higher components including IVGDR (dot-dashed line), respectively. (b) Results for $E_x = 23.5$ MeV.

used in the calculations [26–28]. Transition potentials were constructed by folding the transition densities with an effective α–N interaction [29]:

$$\begin{aligned} V\left(|\vec{r} - \vec{r}\,'|, \rho_0(r')\right) &= -V\left(1 + \beta_V \rho_0^{2/3}(r')\right) e^{-|\vec{r}-\vec{r}\,'|^2/\alpha_V} \\ &\quad - iW\left(1 + \beta_W \rho_0^{2/3}(r')\right) e^{-|\vec{r}-\vec{r}\,'|^2/\alpha_W}, \end{aligned} \tag{5}$$

where $\rho_0(r')$ is the ground-state density. The parameters of the α–N interaction used in the calculations were obtained from fits to the elastic-scattering cross sections measured in a separate experiment and are: $V = 26.7$ MeV, $W = 15.5$ MeV, $\alpha_V = \alpha_W = 4.4$ fm^2 and $\beta_V = \beta_W = -1.9$ fm^2. To calculate the cross section of the isovector giant dipole resonance (IVGDR) excited in the (α, α') reaction at the high bombarding energy of 400 MeV through the Coulomb interaction, photo-absorption data [30] were used in conjunction with DWBA calculations on the basis of the

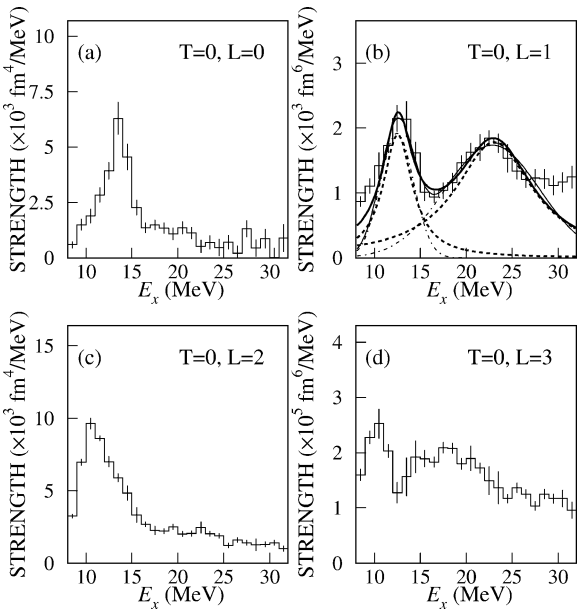

Fig. 3. Strength distributions for the $L = 0, 1, 2$ and 3 transitions in ^{208}Pb, (a) ISGMR, (b) ISGDR, (c) ISGQR and (d) HEOR. The errors shown for each excitation-energy bin were estimated by changing the parameter for one component in order to satisfy $\Delta\chi^2 = 1$ when the fits were performed by the other parameters. The fits to the ISGDR strength distribution for $10 < E_x < 28$ MeV are superimposed. The thick-solid and thick-dashed curves are the results with two Breit–Wigner functions, and the thin-solid and thin-dash-dotted curves are the results with two Gaussian functions.

Goldhaber–Teller model. The contribution of IVGDR was subtracted prior to multipole decomposition of the measured cross sections, carried out in the excitation energy region from $E_x = 8$ MeV to 32 MeV, with the transferred angular momenta up to $L = 13$ taken into account. The results of the fits are shown in Fig. 2 for two 1 MeV energy bins. The strength distributions extracted from these fits for the $L = 0$ (ISGMR), $L = 1$ (ISGDR), $L = 2$ (ISGQR) and $L = 3$ (HEOR) in ^{208}Pb are shown in Fig. 3.

The ISGDR strength clearly has two distinct components. This "bi-modal" ISGDR strength distribution is very interesting. The low-energy component of the ISGDR, near the energy of the ISGMR and IVGDR, has now been observed in several nuclei [8]. It also appears in several of the more recent calculations of the ISGDR strength (see, for example, Refs. [11–16]). However, all the cited calculations clearly establish that only the high-energy (HE) component depends

Table 1
Centroid energies (m_1/m_0), widths (Γ), and EWSR fractions for ISGMR and ISGDR. Numbers in parentheses are obtained from the Gaussian fits

	m_1/m_0 (MeV)	Γ (MeV)	EWSR (%)
ISGMR	13.5 ± 0.2	3.6 ± 0.4	76 ± 5
	(13.5 ± 0.2)	(4.2 ± 0.3)	(58 ± 3)
ISGDR (HE)	23.0 ± 0.3	10.3 ± 0.1	117 ± 3
	(22.5 ± 0.3)	(10.9 ± 0.9)	(107 ± 7)
ISGDR (LE)	12.7 ± 0.2	3.5 ± 0.4	28 ± 1
	(12.5 ± 0.3)	(4.4 ± 0.5)	(21 ± 1)

on the value of nuclear incompressibility employed in the calculations; the position of the low-energy (LE) component is completely independent of the nuclear incompressibility, pointing to its "non-bulk" origin. Further, Vretenar et al. have identified the dynamics of this mode as resulting from surface effects, and have proposed that it arises from a toroidal vibrational mode [14]. The observed centroid for this LE component ($E_x = 12.5 \pm 0.4$ MeV) is higher than the theoretical predictions by several MeV. Incidentally, this is not the expected $1\hbar\omega$ component of the ISGDR, discussed in detail previously by Poelhekken et al. [31]; the $1\hbar\omega$ strength, exhausting 15% of the EWSR for the ISGDR, lies below the low-excitation-energy limit of our experiment.

To determine the centroid energy of the ISGDR, which is derived according to the definition: $E_x = m_1/m_0$ [$m_0 = \sum S_L(E_x)$], the experimental strength distribution was fitted with two Breit–Wigner functions and with two Gaussian functions. The centroid energy, width and EWSR fraction for the ISGDR from both fits are listed in Table 1, together with results for the ISGMR. In the case of the Breit–Wigner fits, the EWSR fraction for the ISGMR is close to 100%, while the EWSR fraction for the ISGDR strength exhausted by the HE component ($\sim 120\%$) is larger than expected ($\sim 85\%$) [28,31]. In the case of the Gaussian fits, on the other hand, the EWSR fraction for the ISGMR is much smaller than 100% (only 60%), and the EWSR fraction for the LE- and HE-ISGDR are 20% and 110%, respectively. We concentrate our discussion in the following on the results with the Breit–Wigner fits.

The errors quoted for the EWSR fractions are only statistical. The systematic errors for the HE

component of the ISGDR are estimated to be large due to $L = 1$ contribution in the continuum, especially at high excitation energies ($28 < E_x < 32$ MeV), which might result from processes unaccounted for in our analysis (for example, quasi-free scattering and second-order effects).

In general, the treatment of "background" has always been the largest source of errors in giant resonance studies with inelastic scattering. In our measurements, we have nearly completely eliminated the "non-physical" component of the background, and treated the physical continuum as composed of a combination of various multipoles. A complication in this approach arises from the possible mimicking of $L = 1$ strength by other processes, as described above. In other approaches, used in some of the previous studies, a "reasonable" background is subtracted from the spectra, prior to multipole decomposition [8,23]. The problem with this method lies in the nature of the background-subtraction procedure itself since it is not possible to calculate the shape and magnitude of the continuum. Regardless, in analyzing our data, we find that the extracted ISGDR positions and widths of the aforementioned LE and HE peaks are nearly identical in both types of the analysis. Indeed, even if we assume the background shape as $\sqrt{E_x - S_{n(p)}}$ ($S_{n(p)}$ is the particle threshold energy) and subtract all the high-energy continuum, the centroid energy shifts down only by 0.6 MeV. The Gaussian fit after subtracting the "physical background" yields a centroid energy of 21.9 ± 0.3 MeV, which approaches a little to the previous results in Refs. [4,5,8]. However, the extracted percentage of the EWSR fraction for the ISGDR reduces to 50%.

In addition to the treatment of the physical continuum, uncertainties in extracted EWSR fractions come from the DWBA calculations, such as the potentials extracted from elastic-scattering data and the energy dependence of the transition density [15,29]. It is, therefore, prudent to assume uncertainties of at least 30% in the quoted EWSR fractions.

Another independent and different approach was used to visualize the peak for the ISGDR. Since the cross section of the ISGDR rapidly decreases from 1° to 2.8°, while those of the HEOR and all higher multipoles and quasi-free scattering are more or less constant in this angular range, the "difference-of-spectra" technique [7] has been employed as shown in Fig. 4. A peak for HE-ISGDR is clearly visible in the difference spectrum obtained by subtracting the spectrum at 2.83° from that at 1.02°. The peak energy for the HE-component of the ISGDR at $E_x \sim 21.6$ MeV is consistent with the results of the present MDA.

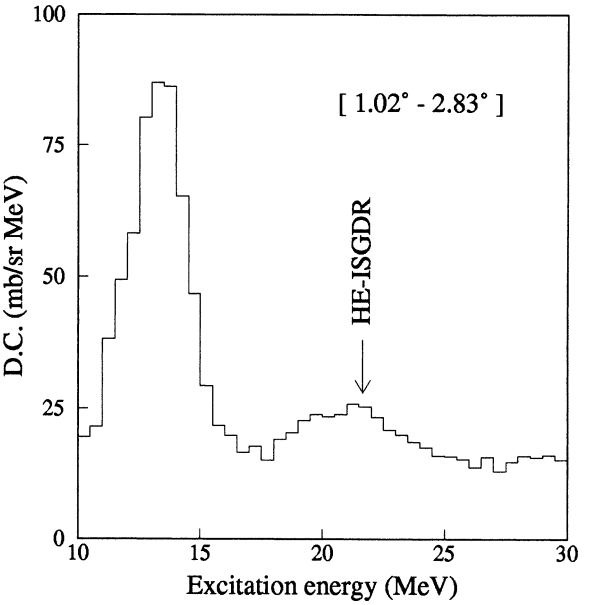

Fig. 4. Difference spectrum obtained by subtracting the spectrum at 2.83° from that at 1.02°. The peak position for the HE-ISGDR (~ 21.6 MeV) is clearly visible. "D.C." referes to the difference in cross sections.

Using the energy of the HE-ISGDR peak ($E_x = 23.0 \pm 0.3$ MeV), one obtains $K_A = 130 \pm 5$ MeV from Eq. (2). On the other hand, using the ISGMR energy ($E_x = 13.5 \pm 0.2$ MeV) in Eq. (1), the K_A value of 134 ± 4 MeV is obtained. These values are very close, providing a consistency between the two compressional modes that has been elusive so far. Indeed, the K_A derived from the ISGDR was reported in the past to be up to 40% lower than that obtained from the ISGMR [9].

Blaizot [32] has provided an empirical relationship between K_A and $K_{\rm nm}$ for ^{208}Pb:

$$K_A = 0.64 K_{\rm nm} - 3.5. \tag{6}$$

With the K_A (~ 130 MeV) obtained from our results, this relation would imply $K_{\rm nm} \sim 210$ MeV.

As mentioned earlier, the well-accepted procedure for extracting $K_{\rm nm}$ from energies of the compressional

Table 2
Centroid energies of ISGDR and ISGMR for ^{208}Pb

	E_{ISGDR} (MeV)		E_{ISGMR} (MeV)	K_{nm} (MeV)
	HE	LE		
This work (Breit–Wigner)	23.0 ± 0.3	12.7 ± 0.2	13.5 ± 0.2	
This work (Gaussian)	22.5 ± 0.3	12.5 ± 0.3	13.5 ± 0.2	
Morsch et al. [4]	21.3 ± 0.8	–	13.8	
Djalali et al. [5]	21.5 ± 0.2	–	13.9	
Adams et al. [6]	22.6 ± 0.2	–	–	
Davis et al. [7]	22.4 ± 0.5	–	–	
Clark et al. [8]	19.9 ± 0.8	12.2 ± 0.6	14.17 ± 0.28	
Hamamoto et al. [11,33]	23.4	~ 14	14.1	217
Colò et al. [12]	23.9 (22.9[a])	10.9	14.1	215
Piekarewicz [13]	24.4	~ 8	13.1	224
Vretenar et al. [14,34]	26.01	10.4	14.1	271
Shlomo and Sanzhur [15]	~ 25.0	~ 15	14.48	230
Gorelik and Urin [16]	22.7	11.1	14.3	–

[a] Including effects of continuum and $2p$–$2h$ coupling [35].

modes involves comparison of the experimental energies with those calculated using suitable effective interactions that have different nuclear incompressibilities. Table 2 lists the present experimental results compared with previously published results and with theoretical calculations. Prior to our measurements, it appeared that all calculations, using nuclear incompressibilities that reproduced the experimental ISGMR energies very well, overestimated the excitation energy of the ISGDR by several MeV [8]. With the results presented herein, this problem has been resolved. With the virtually "background-free" spectra obtained in our work, it has been possible to identify the ISGDR strength up to $E_x \sim 30$ MeV and the centroid of the experimental HE-ISGDR strength determined for ^{208}Pb is now very close to the theoretical predictions. Most of these calculations employ the interactions that give K_{nm} in the range of 215–225 MeV. It may be concluded, therefore, that a value of $K_{\mathrm{nm}} \sim 220$ MeV is consistent with the observed properties of both the compressional modes in ^{208}Pb.

In summary, we have performed $^{208}\mathrm{Pb}(\alpha, \alpha')$ measurements at 400 MeV to study the ISGDR. Energy spectra for (α, α') were obtained without any instrumental background. Using a multipole decomposition analysis, the strength distribution of the ISGDR was obtained up to $E_x \sim 30$ MeV. The ISGDR strength distribution has two components; however, only the high-excitation energy component corresponds to the compressional mode. With our results, both the ISGMR and the ISGDR provide a consistent value of the incompressibility of infinite nuclear matter.

Acknowledgements

The authors acknowledge the staff of the RCNP ring cyclotron for providing a halo-free beam during the experiment. This work was comprised of a series of experiments (E112, E133, E142 and E151) performed at RCNP and supported in part by the US–Japan Cooperative Science Program of the JSPS, and the US National Science Foundation (grants number INT-9910015 and PHY-9901133), and the University of Notre Dame.

References

[1] M.N. Harakeh, et al., Phys. Rev. Lett. 38 (1977) 676.
[2] D.H. Youngblood, et al., Phys. Rev. Lett. 39 (1977) 1188.
[3] S. Stringari, Phys. Rev. Lett. B 108 (1982) 232.
[4] H.P. Morsch, et al., Phys. Rev. Lett. 45 (1980) 337;
H.P. Morsch, et al., Phys. Rev. C 28 (1983) 1947.
[5] C. Djalali, et al., Nucl. Phys. A 380 (1982) 42.
[6] G.S. Adams, et al., Phys. Rev. C 33 (1986) 2054.
[7] B.F. Davis, et al., Phys. Rev. Lett. 79 (1997) 609.
[8] H.L. Clark, Y.-W. Lui, D.H. Youngblood, Phys. Rev. C 63 (2001) 031301(R).
[9] U. Garg, RIKEN Rev. 23 (1999) 65;
U. Garg, Nucl. Phys. A 649 (1999) 66c.
[10] J.P. Blaizot, Nucl. Phys. A 649 (1999) 61c;
J.P. Blaizot, RIKEN Rev. 23 (1999) 65.

[11] I. Hamamoto, H. Sagawa, X.Z. Zhang, Phys. Rev. C 57 (1998) R1064.
[12] G. Colò, et al., Phys. Lett. B 485 (2000) 362.
[13] J. Pikarewicz, Phys. Rev. C 62 (2000) 051304(R); J. Pikarewicz, Phys. Rev. C 64 (2001) 024307.
[14] D. Vretenar, et al., Phys. Rev. C 65 (2002) 021301(R); D. Vretenar, et al., Phys. Lett. B 487 (2000) 334.
[15] S. Shlomo, A.I. Sanzhur, Phys. Rev. C 65 (2002) 044310.
[16] M.L. Gorelik, M.H. Urin, Phys. Rev. C 64 (2001) 047301.
[17] M. Fujiwara, et al., Nucl. Instrum. Methods Phys. Res. A 422 (1999) 484.
[18] T. Noro, et al., RCNP Annu. Rep. (1991) 177.
[19] Y. Sakemi, et al., Phys. Rev. C 51 (1995) 3162.
[20] A. Tamii, et al., Phys. Lett. B 459 (1999) 61.
[21] T. Kawabata, et al., Phys. Rev. C 65 (2002) 064316.
[22] M. Itoh, et al., RCNP Annu. Rep. (1999) 7.
[23] B. Bonin, et al., Nucl. Phys. A 430 (1984) 349.
[24] T. Wakasa, et al., Phys. Rev. C 55 (1997) 2909.
[25] J. Raynal, Program ECIS 95 NEA 0850/14 (1996).
[26] G.R. Satchler, Nucl. Phys. A 472 (1987) 215.
[27] M.N. Harakeh, A.E.L. Dieperink, Phys. Rev. C 23 (1981) 2329.
[28] M.N. Harakeh, A. van der Woude, Giant Resonances: Fundamental High-Frequency Modes of Nuclear Excitation, Oxford Univ. Press, Oxford, 2001.
[29] A. Kolomiets, O. Pochivalov, S. Shlomo, Phys. Rev. C 61 (2000) 034312.
[30] B.L. Berman, S.C. Fultz, Rev. Mod. Phys. 47 (1975) 712.
[31] T.D. Poelhekken, et al., Phys. Lett. B 278 (1992) 423.
[32] J.P. Blaizot, et al., Nucl. Phys. A 591 (1995) 435.
[33] I. Hamamoto, H. Sagawa, X.Z. Zhang, Phys. Rev. C 56 (1997) 3121.
[34] D. Vretenar, et al., Nucl. Phys. A 621 (1997) 853.
[35] G. Colò, et al., RIKEN Rev. 23 (1999) 39, and private communication.